CHEMISTRY OF MATERIALS

Article

pubs.acs.org/cm

Atomic-Resolution Visualization of Distinctive Chemical Mixing Behavior of Ni, Co, and Mn with Li in Layered Lithium Transition-Metal Oxide Cathode Materials

Pengfei Yan,[†] Jianming Zheng,[‡] Dongping Lv,[‡] Yi Wei,[§] Jiaxin Zheng,[§] Zhiguo Wang,[∥] Saravanan Kuppan,[⊥] Jianguo Yu,[#] Langli Luo,[†] Danny Edwards,[‡] Matthew Olszta,[‡] Khalil Amine,[¶] Jun Liu,[‡] Jie Xiao,[‡] Feng Pan,[§] Guoying Chen,[⊥] Ji-Guang Zhang,*[,‡] and Chong-Min Wang*[,†]

[†]Environmental Molecular Sciences Laboratory and [‡]Energy and Environmental Directorate, Pacific Northwest National Laboratory, 902 Battelle Boulevard, Richland, Washington 99352, United States

[§]School of Advanced Materials, Shenzhen Graduate School, Peking University, Shenzhen 518055, People's Republic of China

[∥]Department of Applied Physics, University of Electronic Science and Technology of China, Chengdu, 610054, People's Republic of China

[⊥]Environmental Energy Technologies Division, Lawrence Berkeley National Laboratory, Berkeley, California 94720, United States

[#]Center for Advanced Modeling and Simulation, Idaho National Laboratory, Idaho Falls, Idaho 83415, United States

[¶]Chemical Sciences and Engineering Division, Argonne National Laboratory, 9700 South Cass Avenue, Argonne, Illinois 60439, United States

Supporting Information

ABSTRACT: Capacity and voltage fading of layered structured cathode based on lithium transition-metal oxide is closely related to the lattice position and migration behavior of the transition-metal ions. However, it is scarcely clear about the behavior of each of these transition-metal ions in this category of cathode material. We report direct atomic resolution visualization of interatomic layer mixing of transition metals (Ni, Co, Mn) and lithium ions in layered structured oxide cathodes for lithium-ion batteries. Using chemical imaging with an aberration-corrected scanning transmission electron microscope (STEM) and density function theory calculations, we discovered that, in the layered cathodes, Mn and Co tend to reside almost exclusively at the lattice site of transition-metal (TM) layer in the structure or little interlayer mixing with Li. In contrast, Ni shows a high degree of interlayer mixing with Li. The fraction of Ni ions resides in the Li layer followed by a near linear dependence on total Ni concentration before reaching saturation. The observed distinctively different behavior of Ni with respect to Co and Mn provides new insights on both capacity and voltage fade in this class of cathode materials based on lithium and TM oxides, therefore providing scientific basis for selective tailoring of oxide cathode materials for enhanced performance.

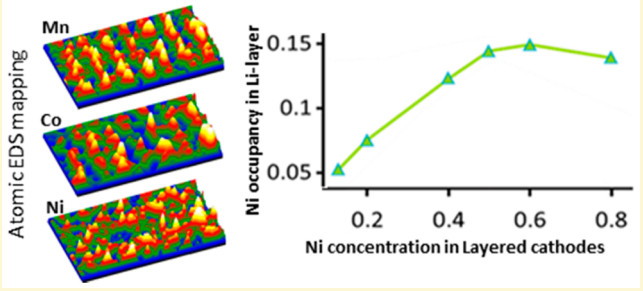

1. INTRODUCTION

Layered lithium transition-metal (TM) oxides as cathode materials for lithium-ion batteries (LIBs) have attracted extensive investigations due to their high-energy density which is critical for mobile energy storage such as portable electronics and electrical vehicle applications.[1−10] Their unique crystallographic structure, Li layer and TM-rich layer stacked alternatively with an oxygen layer, enables a fast two-dimensional Li-ion diffusion and high theoretical capacity. As most well-known layered cathodes, $LiCoO_2$ has been commercialized for several decades. However, the high cost and safety issues of Co forced the community to seek for alternative elements that are low cost and environmentally benign. Under worldwide concerted efforts in the past decade, new family members of layered cathodes, such as Li−Mn-rich (LMR) and $LiMO_2$ (M = Mn, Co, and Ni) layered cathodes, have been demonstrated to have the potential to meet the high-energy density, low cost, and safety requirements of next-generation LIBs.[11−13] In the new series of layered cathodes, the lattice site position, valence, and coordinate environment of the TM ions and their dynamic behavior and interaction with other ions during the battery operation play a crucial role in battery performance.

Taking Ni as an example, it has been found that Ni plays many conflicting roles in controlling cathode performance. On one hand, Ni substituent in Mn-based layered cathodes not

Received: May 29, 2015
Revised: July 6, 2015

DOI: 10.1021/acs.chemmater.5b02016
Chem. Mater. XXXX, XXX, XXX−XXX

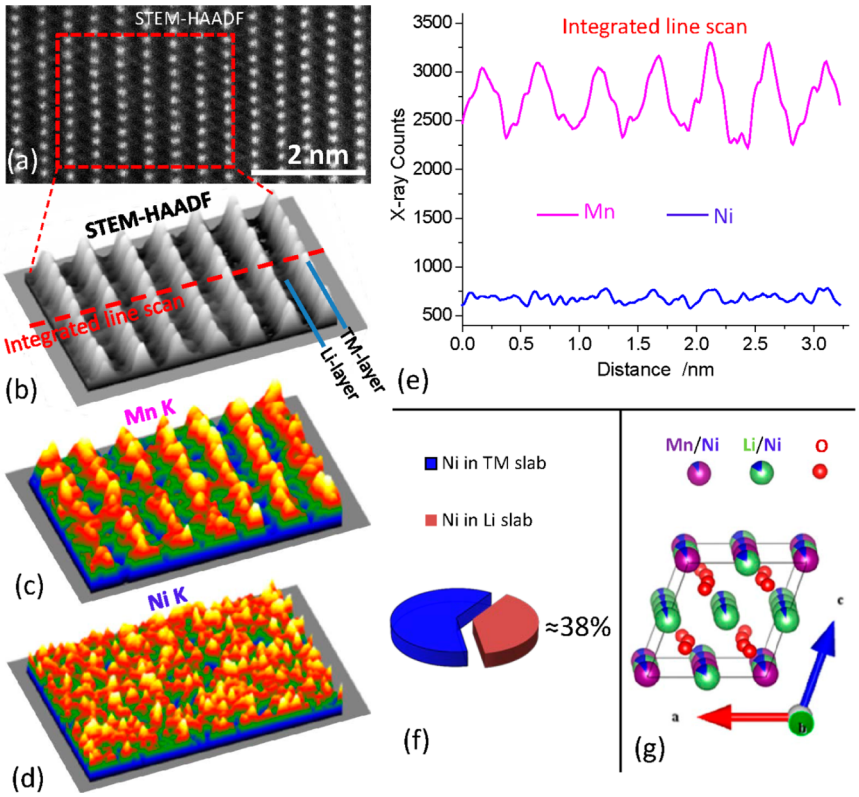

Figure 1. $Li_{1.2}Ni_{0.2}Mn_{0.6}O_2$ (20N-LMR) sample. (a) STEM-HAADF image from the [010] zone axis. (b) EDS mapping region. (c) Surface plot of Mn K map. (d) Surface plot of Ni K map. (e) Integrated line scan profile showing X-ray counts distribution across the layered structure. (f) Based on counts ratio from the TM layer and Li layer, 38% Ni was estimated to seat in the Li layer due to interlayer Li/Ni mixing. (g) Optimized crystal model for 20N-LMR based on EDS mapping results.

only participates in the redox process during charge/discharge but also stabilizes the layered structure.[13−15] On the other hand, Ni can also play detrimental roles. First, during material processing, Ni is prone to segregate at the particle surface to form an electrochemical inactive surface layer in pristine materials.[16−18] Second, it has been observed that, during the battery cycling, Ni further migrates from the bulk lattice to the surface, leading to the gradual formation of a Ni-rich surface layer.[18] Furthermore, the interlayer mixing between Li and Ni, which is the exchange of Li and Ni between TM and Li layers, can directly affect the function of the cathode. Experimental observation indicates that for LMR cathodes higher Li/Ni interlayer mixing leads to better performance than those with lower Li/Ni interlayer mixing.[19] However, theoretical calculations indicate that a high Li/Ni interlayer mixing can result in a smaller Li-layer spacing and consequently high-energy barrier for Li-ion hopping, which may be the main cause of the relatively low rate capability of Ni-contained layered cathodes.[20,21]

For the case of Co, $LiCoO_2$ layered cathode is a well-studied example. It was found that there is negligible interlayer cation mixing between Li layer and Co layer in the $LiCoO_2$. An intuitive explanation for this is the large ionic size difference between Li^+ (0.76 Å) and Co^{3+} (0.545 Å). However, for Ni-containing layered cathodes, the possibility of Li^+/Ni^{2+} exchange is much higher considering the similar ionic size of Ni^{2+} (0.69 Å) and Li^+ (0.76 Å). Therefore, a small portion of Ni can seat in the Li layer, which has been confirmed by both X-ray diffraction (XRD) and neutron diffraction.[19,22−24] Although XRD and neutron diffraction are two well-known methods for determining crystal structure with coordination chemical information, they have inherent limitations on local structure and coordinate chemical information determination. Results from Rietveld refinement of XRD and neutron diffraction patterns are averaged over a large amount of sample, coupled with contributions from many factors that could lead to large errors, especially for nanoscale materials with mixed ions. Particularly for layered cathode materials, XRD and neutron diffraction cannot differentiate the effects originating from surface and grain boundary,[16−18] inhomogeneous composition,[25−27] plane defects (stacking faults and rotation domains),[17,28−31] and particle shape and size (especially for nanoparticles).[10] Transmission electron microscopy, as an alternative approach, is very suitable for local area microanalysis. Advances in scanning transmission electron microscopy (STEM) have made it possible to perform atomic level chemical imaging using STEM-EDS (EDS, energy-dispersive spectroscopy) and STEM-EELS (EELS, electron energy-loss spectroscopy).[32−40]

For the complex lithium transition-metal oxide cathode system, it is far from clear how the TM and Li ions coordinate with each other in the lattice and how their interaction evolve upon battery cycling. Precise and high spatial determination of local atomic information is essential. In this work, for the first time, we use atomic resolution STEM-EDS mapping to probe the local coordinate chemical information in six types of layered cathode materials for LIBs, enabling us to directly visualize and compare the TM element distributions at the atomic level. On the basis of the atomic resolution EDS maps and quantitative analysis, we demonstrate significantly different intermixing

DOI: 10.1021/acs.chemmater.5b02016
Chem. Mater. XXXX, XXX, XXX−XXX

characteristics for Li/Mn, Li/Co, and Li/Ni. The distribution of substituents is not uniform in the Li layers, which may also influence the Li-ion transportation properties during battery cycling. This work provides unprecedented knowledge for correlating atomic structure with battery properties and insights on the role of each TM ion, therefore guiding the smart design of new cathode materials required for advanced LIBs.

2. EXPERIMENTAL SECTION

2.1. Material Synthesis. $Li_{1.2}Ni_{0.2}Mn_{0.6}O_2$ (20N-LMR), $LiNi_{0.5}Mn_{0.5}O_2$ (NM55), and $LiNi_{0.6}Co_{0.2}Mn_{0.2}O_2$ (NCM622) were synthesized via a coprecipitation method. The detailed description of the synthesis procedure has been reported in prior publications.[18,41] $Li_{1.2}Ni_{0.13}Co_{0.13}Mn_{0.54}O_2$ (NC-LMR) was synthesized by using a molten salt method as described in a previous publication.[42] $LiNi_{0.4}Co_{0.2}Mn_{0.4}O_2$ (NCM424) and $LiNi_{0.8}Co_{0.15}Al_{0.05}O_2$ (NCA)) are commercially available materials manufactured by TODA KOGYO company (provided by CAMP Facility at Argonne National Laboratory).

2.2. Material Characterization. The six layered cathodes were investigated by a JEOL JEM-ARM200CF microscope which is operated at 200 kV. This microscope is equipped with a probe spherical aberration corrector and a JEOL SDD detector with a 100 mm^2 X-ray sensor, enabling subangstrom resolution in STEM mode and highly efficient X-ray collections that are 10 times faster than a traditional detector with excellent noise-to-signal ratio, respectively. For the STEM-HAADF (HAADF, high-angle annular dark-field) imaging, the inner and outer collection angles of an annular dark field detector are 68 and 280 mrad, respectively. For atomic level EDS mapping, signal was collected by scanning the same region multiple times with dwell time of 0.1 ms. The frame size for all four samples were 128 × 96 pixels. The probe current was minimized to 11 pA to suppress possible beam-induced damage. The EDS data were collected and processed by using Analysis Station 3.8.0.52 (JEOL Engineering Co., Ltd.). The EDS images presented in this work were plotted using DigitalMicrograph (Gatan Inc., Version 2.30.542.0) with the surface plot function.

2.3. DFT Calculations. All calculations are performed using the plane-wave projector-augmented wave method[43,44] with an energy cutoff of 450 eV, as implemented in the Vienna ab initio simulation package. The Perdew−Burke−Ernzerhof (PBE) form[45] of generalized gradient approximation is chosen as the exchange-correlation potential. The PBE+U approach[46] is employed to take account of the strong on-site Coulomb interaction (U) presented in the localized 3d electrons of Mn, Co, and Ni, with the U values set to 3.5, 3.3, and 6.4 eV for them, respectively. All the layered structures are fully relaxed and optimized to their energetically favorable structure. Antiferromagnetic structure is applied in these structures to obtain their minimum energy structure.[47] We build a supercell comprised by 5 × 2 unit cells containing 30 formula units with the prototypical $R\bar{3}m$ layer structure. The percentage of exchange defects is 3.3%. K-points array is set as 4 × 4 × 2 for sampling Brillouin zone.

3. RESULTS AND DISCUSSION

3.1. Selective Atomic Mixing of Ni, Co, and Mn with Li in Li Layer−LMR Cathodes. Two LMR cathodes, $Li_{1.2}Ni_{0.2}Mn_{0.6}O_2$ (20N-LMR) and $Li_{1.2}Ni_{0.13}Co_{0.13}Mn_{0.54}O_2$ (NC-LMR), have been studied. Before EDS mapping was conducted, the two samples were first tilted to [010] zone axis according to the monoclinic $C2/m$ structure. To achieve atomic level EDS mapping, each atomic column must be well-resolved in STEM-HAADF imaging. Figure 1a is a typical STEM-HAADF image, showing good resolution (∼1.1 Å, estimated from fast Fourier transformation). Figure 1b−d shows EDS maps obtained from the region highlighted in (a). Because of smaller image pixels (128 × 96) and shorter dwell time (0.1 ms), the STEM-HAADF image obtained in EDS mapping (Figure 1b) has relatively poor resolution, but the layered structure is clearly resolved. The distribution of Mn and Ni was shown in parts (c) and (d), respectively, of Figure 1. The Mn map clearly reveals that Mn ions mainly reside in the TM layers while the Ni map shows a rather random distribution. Even though parts (c) and (d) of Figure 1 are showing relative intensity distribution, we still can conclude that there is a considerable amount of Ni in the Li layers. Thus, with atomic level EDS mapping, for the first time, we directly visualized the interlayer mixing of Ni ions in the layered oxide cathode. By summation of the signal counts along the layer direction, an integrated line scan profile with direction perpendicular to the layers is shown in Figure 1e.

Quantitative STEM-EDS analysis is based on the Cliff-Lorimer method. For a binary alloy A−B the X-ray peak intensities I_A and I_B are related to the concentrations of C_A and C_B in wt % by the relationship

$$\frac{C_A}{C_B} = k_{AB}\frac{I_A}{I_B} \text{ and } k_{AB} = \frac{k_{ASi}}{k_{BSi}}$$

where k_{ASi} and k_{BSi} are the ratio factors for the chemical systems of A and B, respectively, with silicon. These factors are not constants. In the current work, for each EDS mapping series the sample thickness is very similar and other experimental conditions were kept as the same. Therefore, we can sum up each element X-ray counts from TM layers and Li layers separately and apply the Cliff-Lorimer method to calculate their concentration ratios in TM layers and Li layers. However, because of a variety of factors, the electron beam will spread while going through the specimen. Therefore, even with subangstrom probe size of the beam, the collected EDS signal from STEM-EDS still suffers contributions from neighboring atom columns. Thus, for example, in Figure 1e considerable Mn X-ray signal was detected from Li layers, even though negligible Mn is residing there according to previous XRD and neutron diffraction analysis.[23] Thus, in Figure 1e, Mn signal counts from Li layers are treated as background noise which comes from neighboring TM layers. Assuming no interlayer mixing between Mn and Li, we used Mn map as the reference to calculate Mn X-ray count ratio between TM layers and Li layers, that is, $R_M = I_{MM}/I_{LM}$ (R_M indicates Mn X-ray ratio and I_{MM} and I_{LM} indicate the total X-ray counts of Mn from TM layers and Li layers, respectively). Such ratio values (R_M) were used to calibrate Ni X-ray counts ratio (R_N) where $R_N = I_{MN}/I_{LN}$ (I_{MN} and I_{LN} indicate the total X-ray counts of Ni from TM layers and Li layers, respectively). Since the Mn map and Ni map were collected simultaneously, the difference between R_M and R_N is a direct result of Mn and Ni distribution difference, that is, the interlayer mixing level difference between Mn/Li and Ni/Li. Taking the background noise level as uniform, we estimated approximately 38% Ni seated in Li layers (Figure 1f). Thus, in 20N-LMR there is around 7.6% (38% × 0.2) Li ions being substituted by Ni in the Li layer; in other words, Ni interlayer mixing level is around 7.6% in 20N-LMR, which is higher than the result of 4.1% deduced from XRD refinement.[19] On the basis of our EDS measurement, a modified crystal model for 20N-LMR cathode is presented in Figure 1g. The calculated Ni value is relative to that of Mn, which makes it more reliable compared to the value estimated from absolute signal counts; as in this case the electron beam propagation effects (channeling, dechanneling, delocaliztion, and scattering

DOI: 10.1021/acs.chemmater.5b02016
Chem. Mater. XXXX, XXX, XXX−XXX

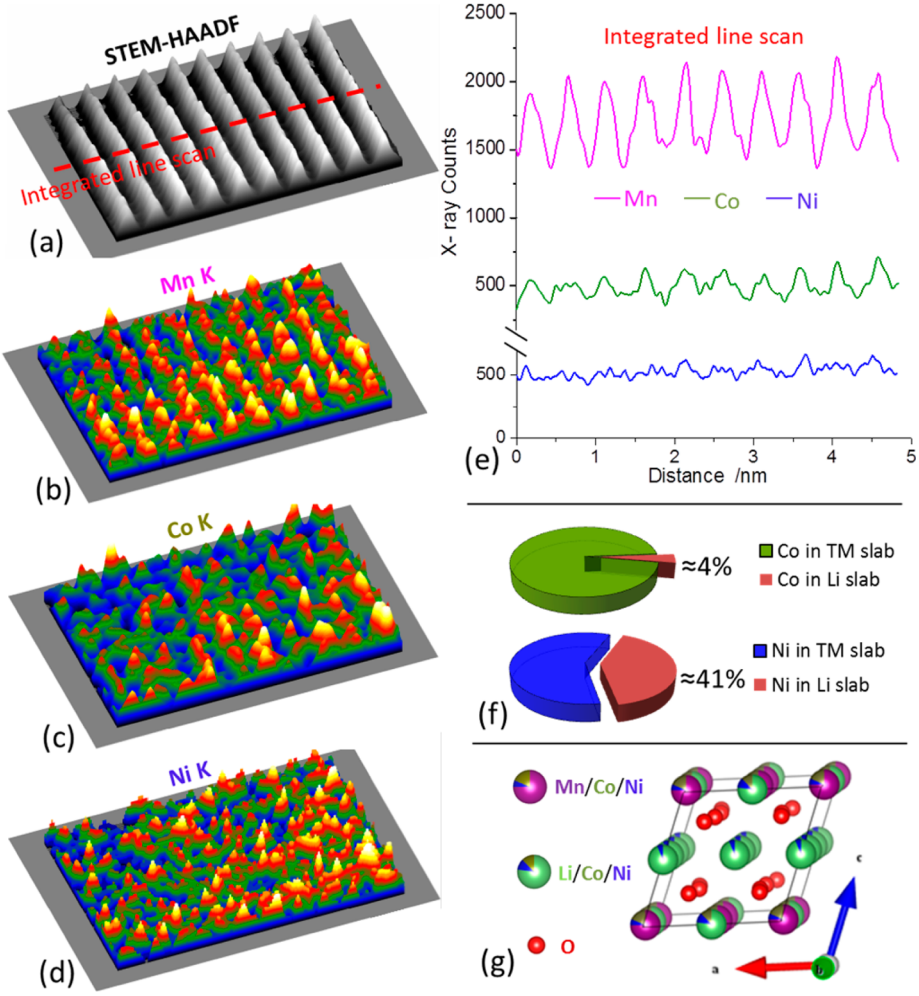

Figure 2. $Li_{1.2}Ni_{0.13}Co_{0.13}Mn_{0.54}O_2$ (NC-LMR) sample. (a) [010] zone axis STEM-HAADF image showing the EDS mapping region. (b) Surface plot of Mn K map. (c) Surface plot of Co K map. (d) Surface plot of Ni K map. (e) Integrated line scan profile showing X-ray counts distribution across the layered structure. (f) On the basis of counts ratio from the TM layer and Li layer, 4% Co and 41% Ni were estimated to seat in the Li layer due to interlayer mixing. (g) Optimized crystal model for NC-LMR based on EDS mapping results.

spread) have been minimized. Detailed calculation method is described in the Supporting Information.

Figure 2 shows the STEM-HAADF image and EDS mapping results for $Li_{1.2}Ni_{0.13}Co_{0.13}Mn_{0.54}O_2$ (NC-LMR) sample. Mn K map (Figure 2b) clearly shows the confinement of this main element in the TM layers. The substituent elements Co and Ni, surprisingly, behave differently. While the Co K map (Figure 2c) shows a well-resolved layered structure, Ni K map (Figure 2d) appears very similar to that observed in the 20N-LMR sample (Figure 1d), revealing a fairly random distribution of Ni. The integrated line scan profile (Figure 2e) provides quantitative X-ray counts for Mn, Co, and Ni, which shows that the total counts for Co and Ni are at a similar level but their profiles are quite different. Again, the Co and Ni interlayer mixing is calculated by setting the profile of Mn as the reference with no interlayer mixing between Mn and Li. As shown in Figure 2f, only 4% Co resides in Li layers while 41% Ni resides in Li layers. Thus, for the NC-LMR cathode, Co has a negligible interlayer mixing, but Ni shows significantly high interlayer mixing. Ni interlayer mixing level is around 5.3% (41% × 0.13) in NC-LMR. A suggested crystal model for NC-LMR is shown in Figure2g.

3.2. Selective Atomic Mixing of Ni, Co, and Mn with Li in Li-Layer–Layered Cathodes with $R\bar{3}m$ Structure. With the increasing ratio between TM and Li, layered cathodes transform from monoclinic $C2/m$ structure into hexagonal $R\bar{3}m$ layered structure. However, in STEM-HAADF imaging conditions, the [100] zone in the $R\bar{3}m$ layered structure is exactly the same as the [010] zone in the $C2/m$ layered structure. For comparison purposes, we tilted the four $R\bar{3}m$ layered cathodes, $LiNi_{0.4}Co_{0.2}Mn_{0.4}O_2$ (NCM424), $LiNi_{0.5}Mn_{0.5}O_2$ (NM55), $LiNi_{0.6}Co_{0.2}Mn_{0.2}O_2$ (NCM622), and $LiNi_{0.8}Co_{0.15}Al_{0.05}O_2$ (NCA), to the [100] zone axis before subsequent EDS mapping. Figure 3a is the STEM-HAADF image of the EDS mapping region for the NCM424 sample, which shows the same layered structure as the LMR cathodes (Figures 1 and 2). Elemental mapping images for Mn, Co, and Ni further confirm the layered structure (Figure 3b–d). The difference between the three maps can be seen in the integrated line scan profiles (Figure 3e), where the Ni profile shows extra peaks in the Li-layer positions (marked by arrows). Using Mn as the baseline, we estimated 4% Co and 31% Ni reside in the Li layers (Figure 3f). Thus, the interlayer mixing level for Ni is about 12.4% (31% × 0.4) and that of Co is about 0.8% (4% × 0.2). The crystal model for NCM424 is shown in Figure 3g. EDS analysis of the NM55 layered cathode suggests the Ni interlayer mixing level is about 14.5% (see Figure S2 in the Supporting Information for details).

DOI: 10.1021/acs.chemmater.5b02016
Chem. Mater. XXXX, XXX, XXX–XXX

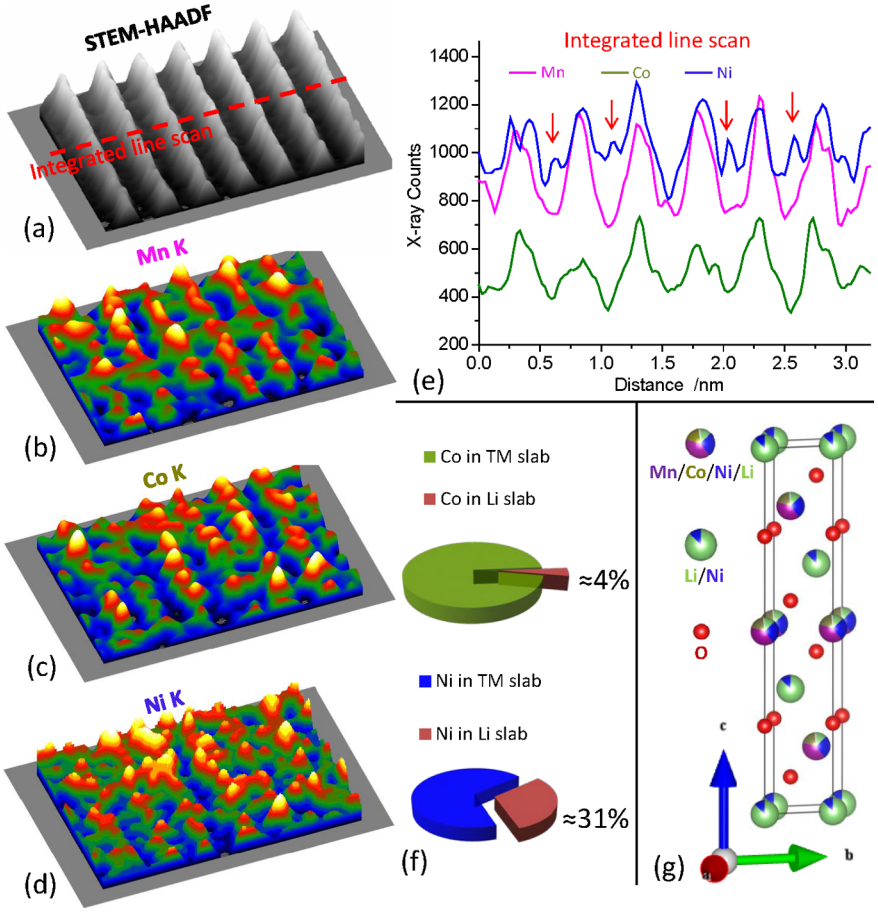

Figure 3. $LiNi_{0.4}Co_{0.2}Mn_{0.4}O_2$ (NCM424) sample. (a) [100] zone axis STEM-HAADF image showing the EDS mapping region. (b) Surface plot of Mn K map. (c) Surface plot of Co K map. (d) Surface plot of Ni K map. (e) Integrated line scan profile showing X-ray counts distribution across the layered structure. Red arrows indicate Ni peak from Li layers. (f) On the basis of counts ratio from the TM layer and Li layer, 4% Co and 31% Ni were estimated to seat in the Li layer due to interlayer mixing. (g) Optimized crystal model for NCM424 based on EDS mapping results.

With further increasing Ni concentration, the layered cathode transformed into a Ni-based structure or Ni-rich layered cathode. Figure 4 shows the EDS mapping results from NCM622, where it shows 6% Co and 25% Ni reside in Li layers. Thus, the Ni interlayer mixing level is about 15% in NCM622. Assuming 6% Co in the Li layer in the NCA sample, Ni interlayer mixing is about 14% (Figure S3). Therefore, it seems the Ni interlayer mixing level does not continue to increase with increasing Ni concentration in the Ni-rich region. It is saturated around 15%, which reveals intriguing behavior of Ni in the layered cathodes.

3.3. New Insights from Atomic Resolution EDS Mapping. Three novel points revealed from the above EDS analysis are discussed below. First of all, Ni, Co, and Mn show significantly different tendencies toward interlayer mixing with Li. Essentially, Mn shows near zero interlayer mixing and Co shows slightly higher interlayer mixing compared to Mn but was often negligible, while Ni shows a much higher tendency toward interlayer mixing. To better understand the different interlayer mixing levels among Li/Ni, Li/Co, and Li/Mn, we performed DFT calculations using NM424 cathode as an example. The antisite defect pairs due to Li/TM interlayer exchange are shown in Figure 5. According to the DFT calculation results (shown in Table 1), Li/Ni antisite defect pairs show much lower total energy increase than those of Li/Co and Li/Mn, which indicates Li/Ni interlayer mixing is the easiest one to make happen, while Li/Co and Li/Mn interlayer mixing are unlikely to occur. Thus, as the two important substituents for Mn-based layered cathodes, Co and Ni are clearly different as far as structural coordination chemistry is concerned. Co behaves similar to Mn and it almost exclusively seats in the TM layers. In contrast, Ni has a relatively weak preference in occupying TM layers, especially at low substitution levels. Such difference may explain the different electrochemical behaviors observed on Co- and Ni-containing cathodes. For example, in LMR cathodes, increasing Co substitution level led to poor performance,[48] while Kim et al. found that increasing the Ni level enhanced cell performance.[15]

Second, our EDS analysis suggested a higher Ni interlayer mixing level as compared to the previous results from XRD and neutron diffraction studies.[19,22,23] As shown in Figure 6, we summarized our EDS measurements and previous published results on Ni interlayer mixing as a function of the total Ni concentration in the oxides. It is amazing that the EDS and XRD yield similar trends with respect to the dependence of Ni interlayer mixing on the total Ni concentration, despite the values from EDS being slightly higher than those from XRD. The main difference observed in the low Ni content range may come from both experimental and analysis methods. First, the physical model used for XRD refinement is incorrect for LMR cathodes. Only $R\bar{3}m$ structure was used as a crystal model in both Fell's work[19] and Lu's work,[22] while in reality, there is a

DOI: 10.1021/acs.chemmater.5b02016
Chem. Mater. XXXX, XXX, XXX−XXX

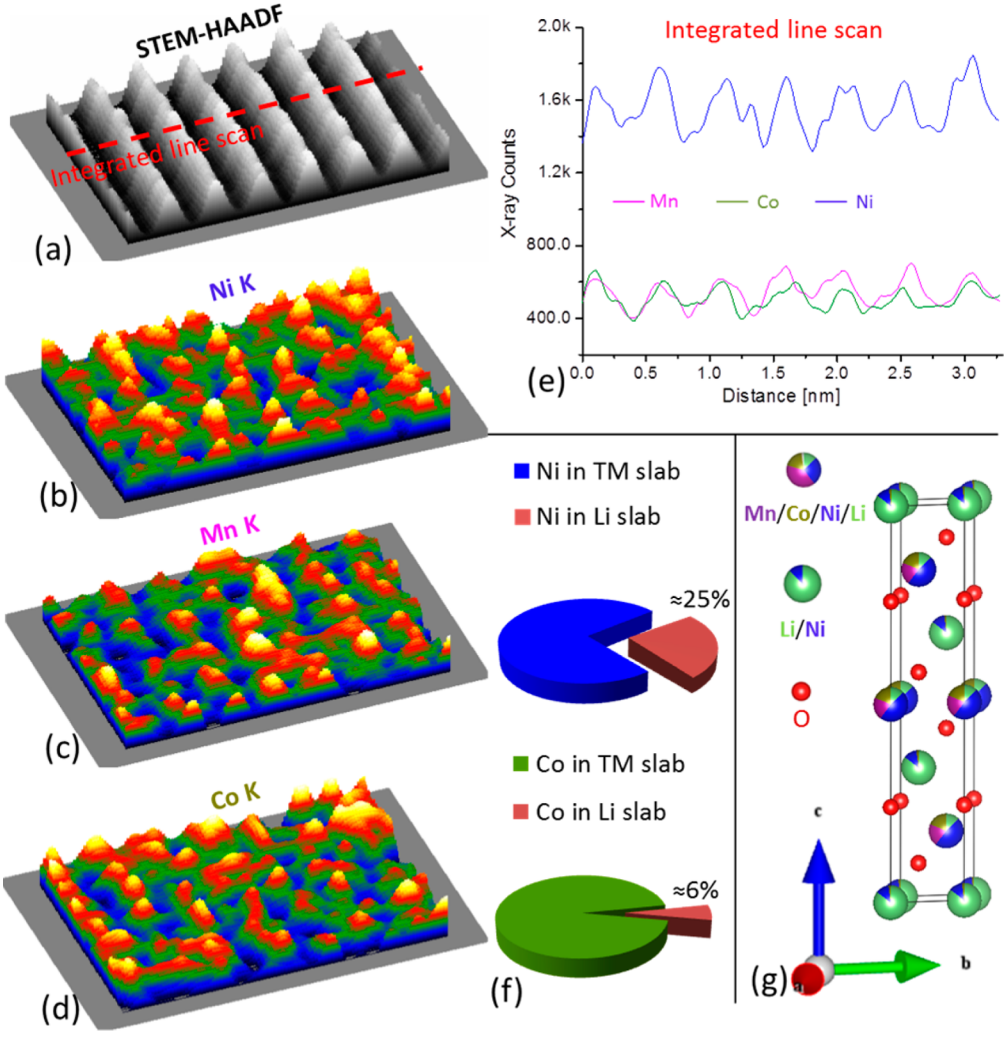

Figure 4. $LiNi_{0.6}Co_{0.2}Mn_{0.2}O_2$ (NCM622) sample. (a) [100] zone axis STEM-HAADF image showing the EDS mapping region. (b) Surface plot of Ni K map. (c) Surface plot of Mn K map. (d) Surface plot of Co K map. (e) Integrated line scan profile showing X-ray counts distribution across the layered structure. (f) 6% Co and 25% Ni were estimated to seat in the Li layer due to interlayer mixing. (g) Optimized crystal model for NCM622 based on EDS mapping results.

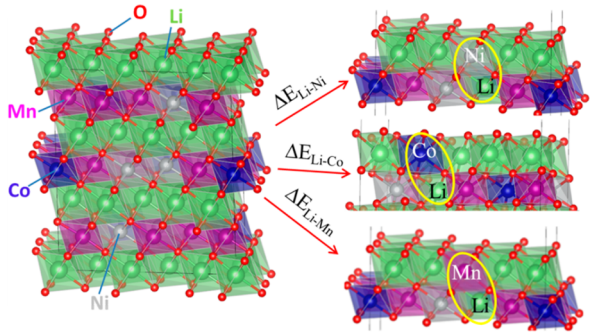

Figure 5. Crystal models showing interlayer exchange of Li/Ni, Li/Co, and Li/Mn in the NCM424 cathode. ΔE indicates total energy increase due to Li/TM exchange.

Table 1. Total Energy Increase for Each Li/TM Antisite Defect Pair and Three Possible Configurations in NCM424 ($LiNi_{0.4}Mn_{0.4}$ $Co_{0.2}O_2$)

total energy increase	Li/Ni exchange	Li/Mn exchange	Li/Co exchange
ΔE	1.374 eV	0.549 eV	0.596 eV

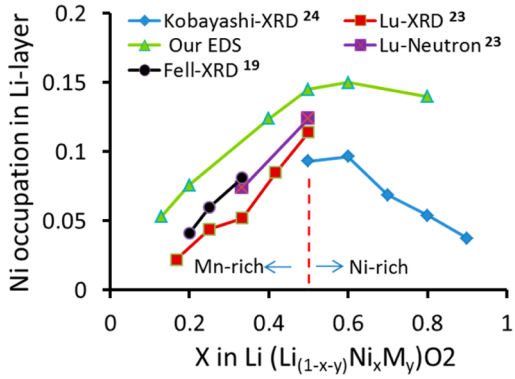

Figure 6. Comparison between our EDS measurement and previous XRD and neutron diffraction measurements on Li/Ni interlayer mixing levels as a function of Ni contents.

large portion of $C2/m$ structure in LMR cathodes.[25,27,31,49] Second, the lower Ni level can increase its uncertainty due to a weaker signal from Ni, which has a similar influence on both EDS and XRD analysis. For the high Ni content cathodes, XRD indicated that Ni interlayer mixing decreases with increasing Ni

DOI: 10.1021/acs.chemmater.5b02016
Chem. Mater. XXXX, XXX, XXX−XXX

content. However, to differ in some way, our EDS results indicate Ni interlayer mixing will reach a saturated level in the Ni-rich region rather than decreasing as suggested by XRD.[24]

The third novel point is that substituent elements are not evenly distributed within bulk lattice. As shown in Figures 1−3) for Mn-rich layered cathodes, even within the nanometer-scale region, Ni and Co both show intensity fluctuation. For Ni-rich layered cathodes in Figures 4 and S3, Mn and Co also show concentration variation on the sub-nanoscale level. Such local composition fluctuation may lead to local lattice distortion and subsequent influence on Li-ion transportation and structure stability. Therefore, crystal models that are based on even distribution of TMs are not in accordance with the real materials, and local composition fluctuation should be considered to better understand cathode behavior.

It has been demonstrated that, upon cycling of $Li_{1.2}Ni_{0.2}Mn_{0.6}O_2$ (20N-LMR) cathode, Ni gradually migrates to the particle surface, leading to Ni depletion in the bulk,[18] structure instability, and consequently cathode voltage and capacity fade. DFT calculations indicated that when Ni resides in the Li layer, the migration barrier for Ni is even lower than that for Li.[16] Apparently, to reduce the migration of Ni to the particle surface during battery operation, the interlayer mixing of Ni into the Li layer should be minimized, which should be taken into consideration during material processing. Furthermore, previous studies indicated that Ni could migrate from the TM layer into the Li layer and result in structure instability.[50,51] However, direct evidence is lacking and its mechanism is also unclear, even though considerable computational work has been carried out.[52−55] Cation migration is the fundamental science for LIBs and demands more efforts along this direction. The present work using atomic resolution EDS chemical imaging provides a new approach. The observation on the drastically different behavior of Ni, Co, and Mn in terms of atomic level mixing indicates that regulating or guiding Ni behavior constitutes one of the crucial steps for mitigating capacity and voltage fade in this class of layer cathode oxides.

4. CONCLUSIONS

For the first time, atomic resolution STEM-EDS mapping was successfully used to probe the structural coordination chemical information, that is, the interlayer mixing between TM and Li in the layered cathodes. Using atomic level mapping, we captured unprecedented and indisputable evidence on the vastly different behaviors of Mn, Co, and Ni toward interlayer mixing with Li. While Mn and Co tend to reside almost exclusively at the lattice site of the TM layer in the structure, Ni shows a significantly higher degree of interlayer mixing with Li layer. The fraction of Ni ions residing in the Li layer has a near linear dependence on the total Ni concentration before reaching saturation in the Ni-rich region. The present atomic level direct observation of distinctively different degrees of selective mixing of Ni, Co, and Mn with Li provides a new way to further understand the electrochemical behavior of LIB cathodes as well as the scientific basis for selective tailoring of new materials with improved performance.

■ ASSOCIATED CONTENT

Supporting Information

The calculation method for quantifying the interlayer mixing levels of Ni and Co, atomic EDS mapping results for NM55 and NCA, and DFT calculations are described in detail. The Supporting Information is available free of charge on the ACS Publications website at DOI: 10.1021/acs.chemmater.5b02016.

■ AUTHOR INFORMATION

Corresponding Authors

*E-mail: jiguang.zhang@pnnl.gov (J.-G.Z.).
*E-mail: Chongmin.wang@pnnl.gov (C.-M.W.).

Notes

The authors declare no competing financial interest.

■ ACKNOWLEDGMENTS

We appreciate the beneficial discussion of Dr. Ping Lu of Sandia National Laboratory and Dr. Anmin Nie from Michigan Technological University during the course of this work. This work was supported by the Assistant Secretary for Energy Efficiency and Renewable Energy, Office of Vehicle Technologies of the U.S. Department of Energy, under contract no. DE-AC02-05CH11231 and subcontract no. 6951379 under the Batteries for Advanced Battery Materials Research (BMR). Part of the STEM-EDS mapping was supported by the Chemical Imaging Initiative at Pacific Northwest National Laboratory (PNNL). The work was conducted in the William R. Wiley Environmental Molecular Sciences Laboratory (EMSL), a national scientific user facility sponsored by DOE's Office of Biological and Environmental Research and located at PNNL. PNNL is operated by Battelle for the Department of Energy under contract no. DE-AC05-76RLO1830. Z.W. was supported by the National Natural Science Foundation of China (11474047). Y.W., J.Z., and F.P. were financially supported by Guangdong Innovation Team Project (no. 2013N080) and Shenzhen Science and Technology Research Grant (nos. ZDSY20130331145131323 and CXZZ20120829172325895).

■ REFERENCES

(1) Tarascon, J. M.; Armand, M. *Issues and challenges facing rechargeable lithium batteries. Nature* **2001**, *414*, 359−367.

(2) Ceder, G.; Chiang, Y. M.; Sadoway, D. R.; Aydinol, M. K.; Jang, Y. I.; Huang, B. *Identification of cathode materials for lithium batteries guided by first-principles calculations. Nature* **1998**, *392*, 694−696.

(3) Sun, Y. K.; Myung, S. T.; Park, B. C.; Prakash, J.; Belharouak, I.; Amine, K. *High-energy cathode material for long-life and safe lithium batteries. Nat. Mater.* **2009**, *8*, 320−324.

(4) Zheng, J.; Gu, M.; Genc, A.; Xiao, J.; Xu, P.; Chen, X.; Zhu, Z.; Zhao, W.; Pullan, L.; Wang, C.; Zhang, J. G. *Mitigating voltage fade in cathode materials by improving the atomic level uniformity of elemental distribution. Nano Lett.* **2014**, *14*, 2628−2635.

(5) Johnson, C. S.; Li, N.; Lefief, C.; Vaughey, J. T.; Thackeray, M. M. *Synthesis, Characterization and Electrochemistry of Lithium Battery Electrodes:xLi2MnO3·(1 −x)LiMn$_{0.333}$Ni$_{0.333}$Co$_{0.333}$O$_2$(0 ≤x≤ 0.7). Chem. Mater.* **2008**, *20*, 6095−6106.

(6) Kim, J. S.; Johnson, C. S.; Vaughey, J. T.; Thackeray, M. M.; Hackney, S. A.; Yoon, W.; Grey, C. P. *Electrochemical and structural properties of xLi$_2$M'O$_3$-(1-x)LiMn$_{0.5}$Ni$_{0.5}$O$_2$ eIectrodes for lithium batteries (M' = Ti, Mn, Zr; 0 ≤ x ≤ 0.3). Chem. Mater.* **2004**, *16*, 1996−2006.

(7) Thackeray, M. M.; Johnson, C. S.; Vaughey, J. T.; Li, N.; Hackney, S. A. *Advances in manganese-oxide 'composite' electrodes for lithium-ion batteries. J. Mater. Chem.* **2005**, *15*, 2257−2267.

(8) Shao-Horn, Y.; Croguennec, L.; Delmas, C.; Nelson, E. C.; O'Keefe, M. A. *Atomic resolution of lithium ions in LiCoO$_2$. Nat. Mater.* **2003**, *2*, 464−467.

(9) Chung, S. Y.; Choi, S. Y.; Kim, T. H.; Lee, S. *Surface-Orientation-Dependent Distribution of Subsurface Cation-Exchange Defects in Olivine-Phosphate Nanocrystals. ACS Nano* **2015**, *9*, 850−859.

DOI: 10.1021/acs.chemmater.5b02016
Chem. Mater. XXXX, XXX, XXX−XXX

(10) Wei, G.-Z.; Lu, X.; Ke, F.-S.; Huang, L.; Li, J.-T.; Wang, Z.-X.; Zhou, Z.-Y.; Sun, S.-G. *Crystal Habit-Tuned Nanoplate Material of $Li[Li_{1/3}-2x/3Ni_xMn_{2/3-x/3}]O_2$ for High-Rate Performance Lithium-Ion Batteries. Adv. Mater.* **2010**, *22*, 4364−4367.

(11) Thackeray, M. M.; Kang, S.-H.; Johnson, C. S.; Vaughey, J. T.; Benedek, R.; Hackney, S. A. *Li_2MnO_3-stabilized $LiMO_2$ (M = Mn, Ni, Co) electrodes for lithium-ion batteries. J. Mater. Chem.* **2007**, *17*, 3112−3125.

(12) Manthiram, A. *Materials Challenges and Opportunities of Lithium Ion Batteries. J. Phys. Chem. Lett.* **2011**, *2*, 176−184.

(13) Croy, J. R.; Gallagher, K. G.; Balasubramanian, M.; Long, B. R.; Thackeray, M. M. *Quantifying Hysteresis and Voltage Fade in xLi_2MnO_3-(1-x)$LiMn_{0.5}Ni_{0.5}O_2$ Electrodes as a Function of Li_2MnO_3 Content. J. Electrochem. Soc.* **2013**, *161*, A318−A325.

(14) Croy, J. R.; Kim, D.; Balasubramanian, M.; Gallagher, K.; Kang, S.-H.; Thackeray, M. M. *Countering the Voltage Decay in High Capacity xLi_2MnO_3-(1−x)$LiMO_2$ Electrodes (M=Mn, Ni, Co) for Li+-Ion Batteries. J. Electrochem. Soc.* **2012**, *159*, A781−A790.

(15) Kim, D.; Croy, J. R.; Thackeray, M. M. *Comments on stabilizing layered manganese oxide electrodes for Li batteries. Electrochem. Commun.* **2013**, *36*, 103−106.

(16) Gu, M.; Belharouak, I.; Genc, A.; Wang, Z.; Wang, D.; Amine, K.; Gao, F.; Zhou, G.; Thevuthasan, S.; Baer, D. R.; Zhang, J. G.; Browning, N. D.; Liu, J.; Wang, C. *Conflicting roles of nickel in controlling cathode performance in lithium ion batteries. Nano Lett.* **2012**, *12*, 5186−5191.

(17) Gu, M.; Genc, A.; Belharouak, I.; Wang, D. P.; Amine, K.; Thevuthasan, S.; Baer, D. R.; Zhang, J. G.; Browning, N. D.; Liu, J.; Wang, C. M. *Nanoscale Phase Separation, Cation Ordering, and Surface Chemistry in Pristine $Li_{1.2}Ni_{0.2}Mn_{0.6}O_2$ for Li-Ion Batteries. Chem. Mater.* **2013**, *25*, 2319−2326.

(18) Yan, P.; Nie, A.; Zheng, J.; Zhou, Y.; Lu, D.; Zhang, X.; Xu, R.; Belharouak, I.; Zu, X.; Xiao, J.; Amine, K.; Liu, J.; Gao, F.; Shahbazian-Yassar, R.; Zhang, J. G.; Wang, C. M. *Evolution of Lattice Structure and Chemical Composition of the Surface Reconstruction Layer in $Li_{1.2}Ni_{0.2}Mn_{0.6}O_2$ Cathode Material for Lithium Ion Batteries. Nano Lett.* **2015**, *15*, 514−522.

(19) Fell, C. R.; Carroll, K. J.; Chi, M.; Meng, Y. S. *Synthesis−Structure−Property Relations in Layered, "Li-excess" Oxides Electrode Materials $Li[Li_{[1/3-2x/3]}Ni_xMn_{[2/3-x/3]}]O_2$ (x=1/3, 1/4, and 1/5). J. Electrochem. Soc.* **2010**, *157*, A1202−A1211.

(20) Kang, K.; Meng, Y. S.; Breger, J.; Grey, C. P.; Ceder, G. *Electrodes with high power and high capacity for rechargeable lithium batteries. Science* **2006**, *311*, 977−980.

(21) Delmas, C.; Pérès, J. P.; Rougier, A.; Demourgues, A.; Weill, F.; Chadwick, A.; Broussely, M.; Perton, F.; Biensan, P.; Willmann, P. *On the behavior of the LixNiO2 system: an electrochemical and structural overview. J. Power Sources* **1997**, *68*, 120−125.

(22) Meng, Y. S.; Ceder, G.; Grey, C. P.; Yoon, W. S.; Jiang, M.; Bréger, J.; Shao-Horn, Y. *Cation Ordering in Layered O3 $Li[Ni_xLi_{1/3-2x/3Mn_{2/3-x/3}}]O_2(0 \leq x \leq 1/2)$ Compounds. Chem. Mater.* **2005**, *17*, 2386−2394.

(23) Lu, Z. H.; Beaulieu, L. Y.; Donaberger, R. A.; Thomas, C. L.; Dahn, J. R. *Synthesis, structure, and electrochemical behavior of $Li[NixLi_{1/3-2x/3}Mn_{2/3-x/3}]O_2$. J. Electrochem. Soc.* **2002**, *149*, A778−A791.

(24) Kobayashi, H.; Sakaebe, H.; Kageyama, H.; Tatsumi, K.; Arachi, Y.; Kamiyama, T. *Changes in the structure and physical properties of the solid solution LiNi1-xMnxO2 with variation in its composition. J. Mater. Chem.* **2003**, *13*, 590−595.

(25) Bareno, J.; Balasubramanian, M.; Kang, S. H.; Wen, J. G.; Lei, C. H.; Pol, S. V.; Petrov, I.; Abraham, D. P. *Long-Range and Local Structure in the Layered Oxide $Li_{1.2}Co_{0.4}Mn_{0.4}O_2$. Chem. Mater.* **2011**, *23*, 2039−2050.

(26) Iddir, H.; Benedek, R. *First-Principles Analysis of Phase Stability in Layered−Layered Composite Cathodes for Lithium-Ion Batteries. Chem. Mater.* **2014**, *26*, 2407−2413.

(27) Yu, X.; Lyu, Y.; Gu, L.; Wu, H.; Bak, S.-M.; Zhou, Y.; Amine, K.; Ehrlich, S. N.; Li, H.; Nam, K.-W.; Yang, X.-Q. Understanding the Rate Capability of High-Energy-Density Li-Rich Layered $Li_{1.2}Ni_{0.15}Co>_{0.1}Mn_{0.55}O_2$ Cathode Materials. *Adv. Energy Mater.* **2014**, *4*, 1300950.

(28) Bareno, J.; Lei, C. H.; Wen, J. G.; Kang, S. H.; Petrov, I.; Abraham, D. P. *Local structure of layered oxide electrode materials for lithium-ion batteries. Adv. Mater.* **2010**, *22*, 1122−1127.

(29) Xu, Z.; Wang, J.; Zhang, K.; Zheng, H.; Dai, Z.-X.; Gui, J.; Yang, X.-Q. Nanoscale Lamellar Monoclinic Li_2MnO_3 Phase with Stacking Disordering in Lithium-Rich and Oxygen-Deficient $Li_{1.07}Mn_{1.93}O_{4-\delta}$ Cathode Materials. *ACS Appl. Mater. Interfaces* **2014**, *6*, 1219−1227.

(30) Jarvis, K. A.; Deng, Z.; Allard, L. F.; Manthiram, A.; Ferreira, P. J. *Understanding structural defects in lithium-rich layered oxide cathodes. J. Mater. Chem.* **2012**, *22*, 11550−11555.

(31) Jarvis, K. A.; Deng, Z. Q.; Allard, L. F.; Manthiram, A.; Ferreira, P. J. *Atomic Structure of a Lithium-Rich Layered Oxide Material for Lithium-Ion Batteries: Evidence of a Solid Solution. Chem. Mater.* **2011**, *23*, 3614−3621.

(32) Okunishi, E.; Sawada, H.; Kondo, Y.; Kersker, M. *Atomic Resolution Elemental Maps by Core Level EELS Using Cs Corrected STEM. Microsc. Microanal.* **2008**, *14*, 1372−1373.

(33) Lu, P.; Romero, E.; Lee, S.; MacManus-Driscoll, J. L.; Jia, Q. *Chemical Quantification of Atomic-Scale EDS Maps under Thin Specimen Conditions. Microsc. Microanal.* **2014**, *20*, 1782−1790.

(34) Itakura, M.; Watanabe, N.; Nishida, M.; Daio, T.; Matsumura, S. *Atomic-Resolution X-ray Energy-Dispersive Spectroscopy Chemical Mapping of Substitutional Dy Atoms in a High-Coercivity Neodymium Magnet. Jpn. J. Appl. Phys.* **2013**, *52*, 050201.

(35) D'Alfonso, A. J.; Freitag, B.; Klenov, D.; Allen, L. J. Atomic-resolution chemical mapping using energy-dispersive x-ray spectroscopy. *Phys. Rev. B: Condens. Matter Mater. Phys.* **2010**, *81*, 100101.

(36) Allen, L. J.; D'Alfonso, A. J.; Freitag, B.; Klenov, D. O. *Chemical mapping at atomic resolution using energy-dispersive x-ray spectroscopy. MRS Bull.* **2012**, *37*, 47−52.

(37) Lu, P.; Xiong, J.; Van Benthem, M.; Jia, Q. *Atomic-scale chemical quantification of oxide interfaces using energy-dispersive X-ray spectroscopy. Appl. Phys. Lett.* **2013**, *102*, 173111.

(38) Sang, X.; Grimley, E. D.; Niu, C.; Irving, D. L.; LeBeau, J. M. *Direct observation of charge mediated lattice distortions in complex oxide solid solutions. Appl. Phys. Lett.* **2015**, *106*, 061913.

(39) Pennycook, S. J.; Varela, M.; Lupini, A. R.; Oxley, M. P.; Chisholm, M. F. *Atomic-resolution spectroscopic imaging: past, present and future. J. Electron Microsc.* **2009**, *58*, 87−97.

(40) Shah, A. B.; Ramasse, Q. M.; Zhai, X. F.; Wen, J. G.; May, S. J.; Petrov, I.; Bhattacharya, A.; Abbamonte, P.; Eckstein, J. N.; Zuo, J. M. *Probing Interfacial Electronic Structures in Atomic Layer $LaMnO_3$ and $SrTiO_3$ Superlattices. Adv. Mater.* **2010**, *22*, 1156−1160.

(41) Zheng, J.; Kan, W. H.; Manthiram, A. *Role of Mn content on the electrochemical properties of nickel-rich layered Li-$Ni_{(0.8-x)}Co_{(0.1)}Mn_{(0.1+x)}O_2$ (0.0 </= x </= 0.08) cathodes for lithium-ion batteries. ACS Appl. Mater. Interfaces* **2015**, *7*, 6926−6934.

(42) Chen, G.; Hai, B.; Shukla, A. K.; Duncan, H. *Impact of Initial Li Content on Kinetics and Stabilities of Layered $Li_{1+x}(Ni_{0.33}Mn_{0.33}Co_{0.33})_{1-x}O_2$. J. Electrochem. Soc.* **2012**, *159*, A1543−A1550.

(43) Blöchl, P. E. *Projector augmented-wave method. Phys. Rev. B: Condens. Matter Mater. Phys.* **1994**, *50*, 17953−17979.

(44) Kresse, G.; Joubert, D. *From ultrasoft pseudopotentials to the projector augmented-wave method. Phys. Rev. B: Condens. Matter Mater. Phys.* **1999**, *59*, 1758−1775.

(45) Perdew, J.; Burke, K.; Ernzerhof, M. *Generalized gradient approximation made simple. Phys. Rev. Lett.* **1996**, *77*, 3865−3868.

(46) Anisimov, V. I.; Zaanen, J.; Andersen, O. K. *Band theory and Mott insulators - Hubbard-U instead of Stoner-I. Phys. Rev. B: Condens. Matter Mater. Phys.* **1991**, *44*, 943−954.

(47) Hwang, B.; Tsai, Y.; Carlier, D.; Ceder, G. *A combined computational/experimental study on $LiNi_{1/3}Co_{1/3}Mn_{1/3}O_2$. Chem. Mater.* **2003**, *15*, 3676−3682.

(48) Xiang, X.; Knight, J. C.; Li, W.; Manthiram, A. *Understanding the Effect of Co3+ Substitution on the Electrochemical Properties of Lithium-*

DOI: 10.1021/acs.chemmater.5b02016
Chem. Mater. XXXX, XXX, XXX−XXX

Rich Layered Oxide Cathodes for Lithium-Ion Batteries. J. Phys. Chem. C **2014**, *118*, 21826−21833.
(49) Yu, H.; Ishikawa, R.; So, Y. G.; Shibata, N.; Kudo, T.; Zhou, H.; Ikuhara, Y. *Direct atomic-resolution observation of two phases in the $Li_{(1.2)}Mn_{(0.567)}Ni_{(0.166)}Co_{(0.067)}O_2$ cathode material for lithium-ion batteries. Angew. Chem., Int. Ed.* **2013**, *52*, 5969−5973.
(50) Nam, K. W.; Bak, S. M.; Hu, E. Y.; Yu, X. Q.; Zhou, Y. N.; Wang, X. J.; Wu, L. J.; Zhu, Y. M.; Chung, K. Y.; Yang, X. Q. *Combining In Situ Synchrotron X-Ray Diffraction and Absorption Techniques with Transmission Electron Microscopy to Study the Origin of Thermal Instability in Overcharged Cathode Materials for Lithium-Ion Batteries. Adv. Funct. Mater.* **2013**, *23*, 1047−1063.
(51) Yabuuchi, N.; Yoshii, K.; Myung, S. T.; Nakai, I.; Komaba, S. *Detailed Studies of a High-Capacity Electrode Material for Rechargeable Batteries, Li_2MnO_3-$LiCo_{1/3}Ni_{1/3}Mn_{1/3}O_2$. J. Am. Chem. Soc.* **2011**, *133*, 4404−4419.
(52) Xu, B.; Fell, C. R.; Chi, M. F.; Meng, Y. S. *Identifying surface structural changes in layered Li-excess nickel manganese oxides in high voltage lithium ion batteries: A joint experimental and theoretical study. Energy Environ. Sci.* **2011**, *4*, 2223−2233.
(53) Reed, J.; Ceder, G.; Van der Ven, A. *Layered-to-spinel phase transition in LixMnO2. Electrochem. Solid-State Lett.* **2001**, *4*, A78−A81.
(54) Qian, D.; Xu, B.; Chi, M.; Meng, Y. S. *Uncovering the roles of oxygen vacancies in cation migration in lithium excess layered oxides. Phys. Chem. Chem. Phys.* **2014**, *16*, 14665−14668.
(55) Carroll, K. J.; Qian, D.; Fell, C.; Calvin, S.; Veith, G. M.; Chi, M.; Baggetto, L.; Meng, Y. S. *Probing the electrode/electrolyte interface in the lithium excess layered oxide $Li_{1.2}Ni_{0.2}Mn_{0.6}O_2$. Phys. Chem. Chem. Phys.* **2013**, *15*, 11128−11138.

DOI: 10.1021/acs.chemmater.5b02016
Chem. Mater. XXXX, XXX, XXX−XXX